CHAPTER 6

RESULT AND DISCUSSION

6.1 Basis Sets

The general procedure to obtain the potential function in analytical form starts with basis set selection. The accuracy outcome and time consumption are the important attributes. The characteristics of various basis sets, examined in this work for Ca(II)-NH_3, are summarized in the Table 6.1.

Table 6.1 Characteristics of basis sets for Ca(II)-NH_3. The interaction energies were evaluated at the optimized Ca(II)-NH_3 configurations. Their orbital exponents and coefficients are summarized in Appendix A.

	Basis Set		without BSSE		with BSSE				
	ammonia	calcium	interaction energy (kcal·mol^{-1})	optimized distances (Å)	interaction energy (kcal·mol^{-1})	optimized distances (Å)	BSSE (kcal·mol^{-1})	NH_3 dipole moment (Debyes)	CPU time (sec)
I	STO-3G	STO-3G	-93.34	2.35	-69.35	2.43	-21.02	1.787	14
II	6-311G**	6-311G**	-62.55	2.40	-59.83	2.44	-2.71	1.768	180
III	DZP	14s/9p/5d	-62.55	2.41	-60.29	2.43	-2.25	1.790	360
IV	14s/9p,3s1p	14s/9p/5d	-62.59	2.40	-61.41	2.42	-1.17	1.914	700

It can be clearly seen, as expected from Table 6.1, that the larger basis sets yield more accurate results and also require more CPU time. A large source of error, both for interaction energies and optimized distances in the SCF calculations, is due to the BSSE. Basis sets **III** and **IV** give similar results, but the CPU time required for basis set **IV** is much higher than for basis set **III**. Basis set **II** is a good choice because it does not consume much CPU time but gives sufficient accuracy. Comparing the basis sets **II** and **III**, no significant difference is found in terms of interaction energy.

However, the error in optimized Ca(II)-NH_3 distance due to the BSSE is lower for the **III** basis set (0.02 Å) than for the **II** basis set (0.04 Å). Note that the CPU time for set **III** is about 2 times longer than for set **II**. In addition, the calculated dipole moment of the ammonia molecules from the first three basis sets is almost the same and is closer to the experimental value of 1.47 Debye [Benedict 1985] compared with that obtained from the **IV** basis set. To compromise among quality, accuracy, CPU time consumption, and memory storage, basis set **III** was selected for use in this work. The remaining error in the NH_3 dipole moment (20%) is believed to be tolerable. However, the BSSE, due to the use of this basis set, was omitted from calculations because of the time consumed, especially in developing the three-body corrections.

6.2 Potential Functions

6.2.1 Pair potentials

As written in Chapter 5, the SCF energies for the Ca(II)-NH_3 interactions were fitted by an analytical function of the form

$$\Delta E_{pair}^{FIT} = \sum_{i=1}^{4}\left[\frac{a_i}{r_i^4}+\frac{b_i}{r_i^3}+c_i\exp(-d_i r_i)+\frac{332.15 q_i q_{Ca}}{r_i}\right] \qquad (6.1)$$

Details of the parameters were described in Chapter 5 and the fitting parameters are shown in Table 6.2.

Table 6.2 Optimized parameters *a, b, c,* and *d* of the analytical pair potential function along with *q* values derived from the *ab initio* calculations (see chapter 5 for details).

	a (kcal.Å^4.mol^{-1})	*b* (kcal.Å^3.mol^{-1})	*c* (kcal.mol^{-1})	*d* (Å^{-1})	*q* (a.u.)
Ca-N	3614.1584	-768.5588	-1083.0971	0.9954	-0.8340
Ca-H	405.7155	173.4295	-3051.4211	2.3356	0.2780

The SCF and fitted energies for some trajectories, including the most favorable configuration where the dipole moment of the ammonia molecule points

away from the ion, are compared in Figure 6.1. This figure indicates good agreement between the SCF two-body and fitted energies, using the parameters given in Table 6.2. The optimal Ca(II)-N distance and the corresponding SCF energy for the most favorable configuration are 2.41 Å and -62.6 kcal.mol^{-1}, respectively.

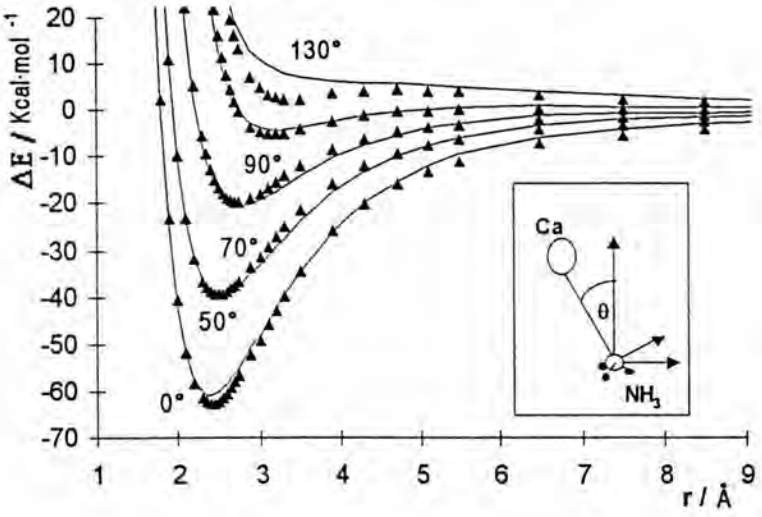

Figure 6.1 Ca(II)-NH_3 interaction energies (kcal·mol^{-1}) obtained from *ab initio* calculations (triangles) and from the best-fit pair potential functions using the fitting parameters given in Table 6.2 (solid lines).

6.2.2 Three-body correction function

The selected analytical form for fitting of the three-body interaction energies described in Chapter 5 is written again as

$$\Delta E_{3-body}^{FIT} = \left\{R_1(r_1)R_2(r_2) + R_1(r_2)R_2(r_1)\right\}\Theta(\theta)\ , \qquad (6.2)$$

where

$$R_1(r_1) = \left(a_0^{(1)} + a_1^{(1)}r_1 + a_2^{(1)}r_1^2 + a_3^{(1)}r_1^3\right)\exp\left(-c_1^{(1)}r_1\right)$$
$$R_2(r_2) = \left(a_0^{(2)} + a_1^{(2)}r_2 + a_2^{(2)}r_2^2 + a_3^{(2)}r_2^3\right)\exp\left(-c_1^{(2)}r_2\right)$$
$$\Theta(\theta) = \left(a_0^{(3)} + a_1^{(3)}\cos\theta + a_2^{(3)}\cos^2\theta + a_3^{(3)}\cos^3\theta\right).$$

The final values of the fitting parameters are summarized in Table 6.3.

Table 6.3 Optimized parameters $a_j^{(i)}$ and $c_j^{(i)}$ of the analytical 3-body correction functions (distances in Å and interaction energies in kcal.mol^{-1}).

	i=1	*i=2*	*i=3*
$a_0^{(i)}$	-26.1335	26.7764	1.8751
$a_1^{(i)}$	-0.0166	-29.0045	-0.8993
$a_2^{(i)}$	0.4367	8.4738	1.8335
$a_3^{(i)}$	0.0303	-0.7836	-0.1777
$c_1^{(i)}$	0.7031	1.0089	-

The SCF three-body interactions, ΔE_{3-body}^{SCF}, and fitted energies, ΔE_{3-body}^{FIT}, are compared in Figure 6.2 where a good coherence between them was demonstrated. Although we can see some data points to the right of the diagonal line, it has been found such points are in configurations where the N1-Ca(II)-N2 angle is over 130° and both ammonia molecules are in the first solvation shell of Ca(II), which never take places in the simulations (Figure 6.17).

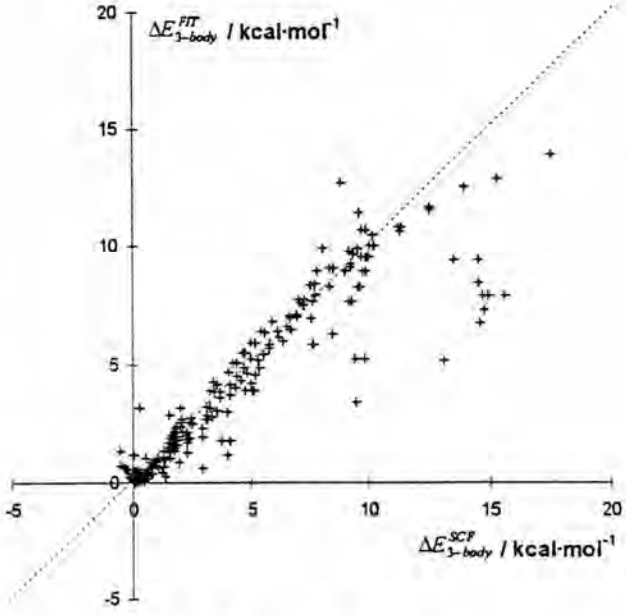

Figure 6.2 Comparison of the three-body interaction energies obtained from the SCF calculations, ΔE_{3-body}^{SCF}, and from the fit, ΔE_{3-body}^{FIT}, for the generated configurations.

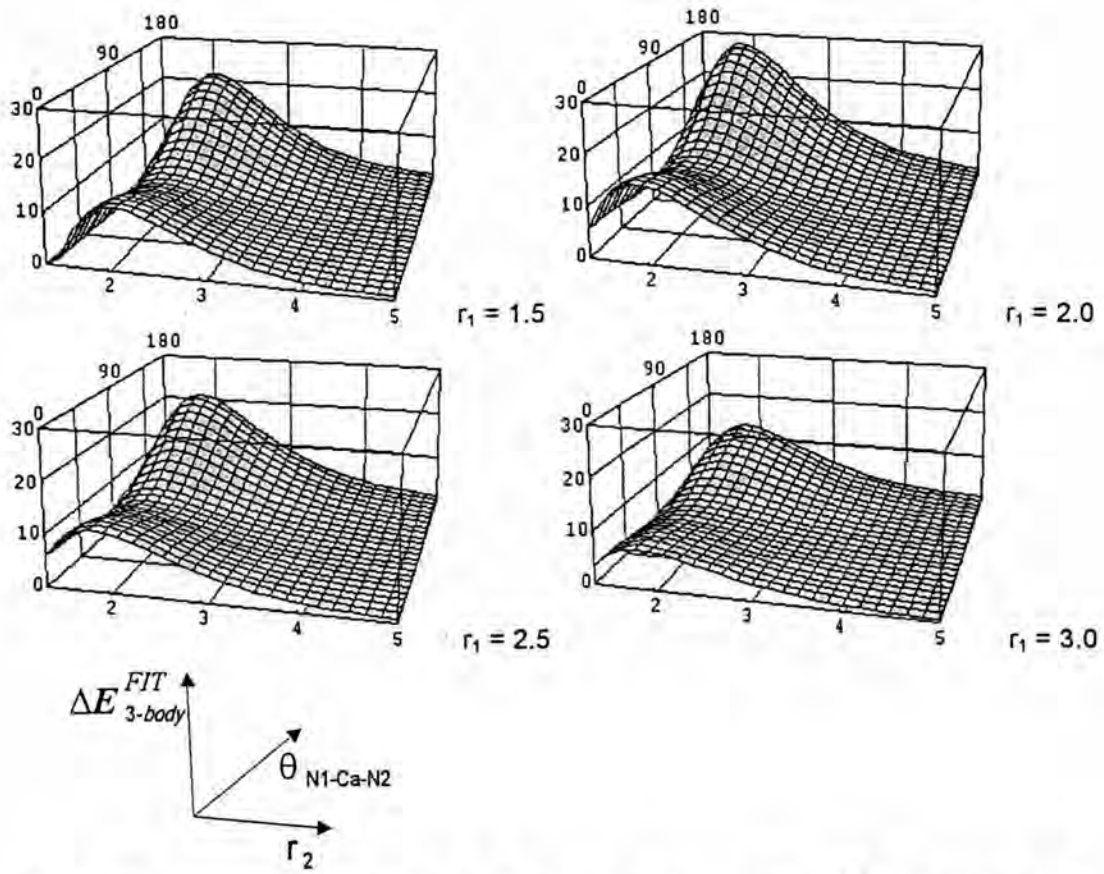

Figure 6.3 Potential energy surface for the three-body correction (ΔE^{FIT}_{3-body} in kcal.mol^{-1}) in the NH_3-Ca(II)-NH_3 complex as a function of the N2-Ca(II) distance (r_2 in Å) and N1-Ca(II)-N2 angle (θ in degrees) at given N1-Ca(II) distances, r_1 = 1.5, 2.0, 2.5, and 3.0 Å (see also Figure 5.2).

Changes of ΔE^{FIT}_{3-body} as a function of the distance between Ca(II) and the two nitrogen atoms, r_1 and r_2, and of the angle between them, θ, can be clearly seen from Figure 6.3. Three-body effects are strong only when the two ammonia molecules are closer than 3 Å from Ca(II), and are negligible when the distance is greater than about 5 Å. All plots in Figure 6.3 show two maxima near $r_2=r_{op}$ and $\theta=0°$ or 180° and a saddle point near $r_2=r_{op}$ and $\theta=90°$, where r_{op} denotes the optimal Ca(II)-N distance in the Ca(II)-NH_3 pair potential. In addition, the three-body energy at $\theta=0°$ shows the strongest repulsion and the three-body energy at $\theta=180°$ is about two times greater than that at $\theta=90°$. Fortunately, the strongest interaction, for $r_2=r_{op}$ and $\theta=0°$, where

the two Ca(II)-N vectors are parallel, cannot occur in the solution. It is interesting to note that among the plots in Figure 6.3, the one with r_1 = 2.0 Å shows the strongest three-body effects. Note also that the three-body correction energies involve only the ammonia molecules in the first solvation shell of Ca(II). In practice, the strongest repulsive effect will be near $r_1 = r_2 = r_{op}$ and $\theta = 180°$. The corresponding value of ΔE^{FIT}_{3-body} is about 10 kcal.mol^{-1}. This is about 20% of the most negative interaction in the Ca(II)-NH_3 pair potential at the same distances.

6.2.3 Pseudopotential effects

In the concentrated solution, to account for free electrons, a pseudopotential was applied to the calculated pair potential as well as the three-body corrections. Three models of pseudopotentials were examined in this work (Chapter 4). The effect of the pseudopotential on the atom-atom pair potential functions is illustrated in Figure 6.4. The direct potential, V_{direct}, plotted in this figure, is directly calculated from the pair potential function (equation 6.1, using the optimal parameters given in Table 6.2). The effective or total potentials, V_{total}, are then calculated from

$$V_{total} = V_{direct} + V_{indirect}, \tag{6.3}$$

where the indirect potential, $V_{indirect}$, is obtained from equation (4.32).

It can be seen from Figure 6.4 that the total potentials become much weaker than the direct potential, both for attractive and repulsive terms, except for model 2. This result, caused by the mutual cancellation of the Coulomb potential and the indirect potential, $V_{indirect}$, is of particular importance for the simulation studies of metal-ammonia solutions. This makes it possible to neglect the treatment of long-range Coulomb interactions by the Ewald or other methods. In contrast, model 2 shows incomplete cancellation; strong interactions are observed even at distances greater than 10 Å, while they are nearly zero for model 1 and 3.

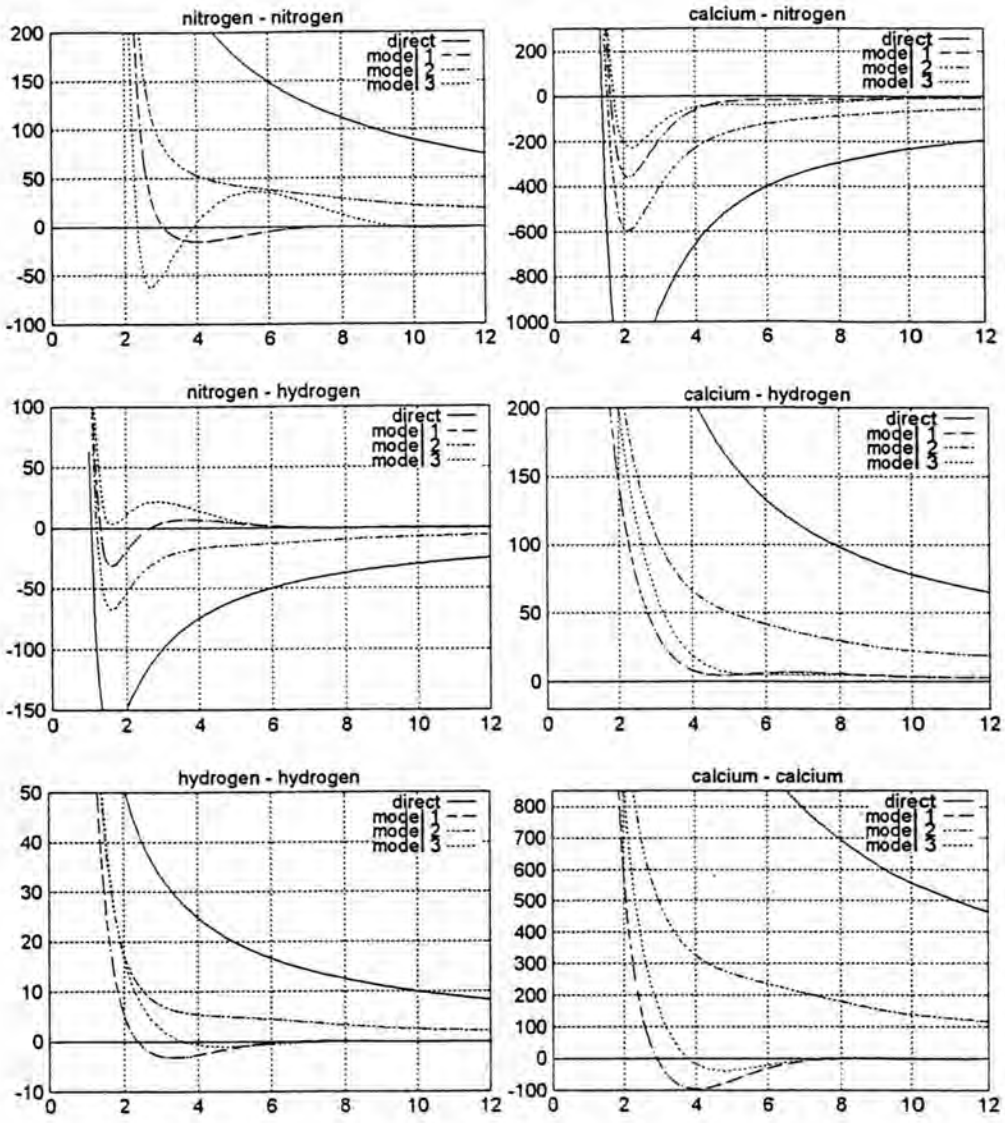

Figure 6.4 The site-site potential vs. distance for the six different interactions in the calcium-ammonia solutions. The full lines denote the direct potential, V_{direct}. The dash-dotted, dashed, and dotted lines denote the total potential, V_{total}, for models 1, 2, and 3, respectively. The energies are in kcal·mol^{-1} and distances in Å.

Although the site-site interactions obtained from model 3 behave similarly to those of model 1, the total ammonia-calcium (Figure 6.5) and ammonia-ammonia (Figure 6.6) interactions are significantly different. The calcium-ammonia interaction of model 3 shows a flat minimum ranging from r ≈ 2.8 to 7.0 Å. In addition, the ammonia-ammonia interaction (Figure 6.6) shows strong, short-range repulsion, and then decays to zero at about 10 Å.

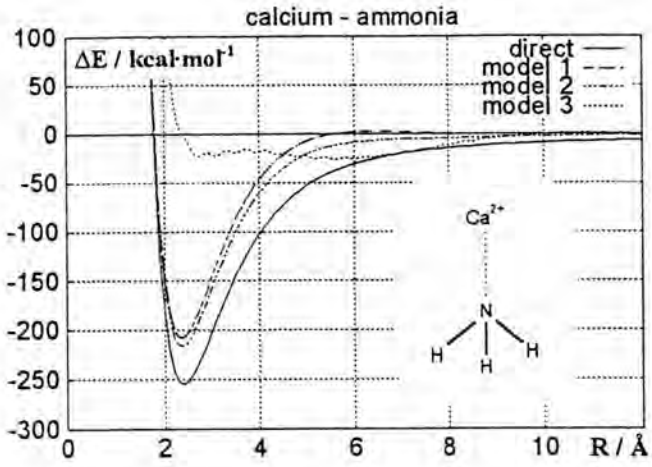

Figure 6.5 Calcium-ammonia pair potential as a function of the calcium-nitrogen distance, for orientations as shown in the insert, at a temperature of 240 K with 7.72 mole percent concentration. The full lines denote the direct potential, V_{direct}. The dash-dotted, dashed, and dotted lines denote the total potential, V_{total}, for models 1, 2, and 3, respectively.

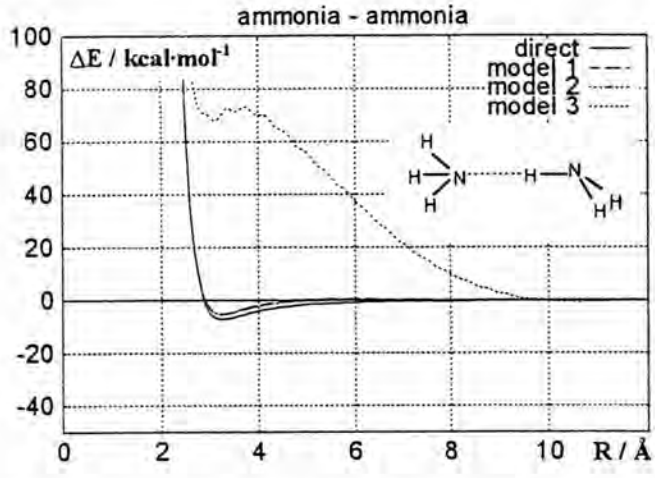

Figure 6.6 Ammonia-ammonia pair potential as a function of nitrogen-nitrogen distance for the insert configuration at 7.72 mole percent concentration. Full lines denote the direct potential, V_{direct}. Dash-dotted, dashed, and dotted lines denote the total potential, V_{total}, for models 1, 2, and 3, respectively.

To monitor the reliability of the pseudopotential, the calcium-calcium pair potential functions were plotted for several concentrations of electrons. The results for the two concentration ranges are displayed in Figure 6.7 and 6.8. At low concentration only a small change in electron density strongly effects the potential function form. In contrast, when the electron density becomes higher than $1x10^{-3}$ electron per $Å^3$ (comparable to 13 Ca(II) ions per 215 NH_3 molecules simulations), a

higher concentration yields only a small change in the potential function, as shown in Figure 6.8.

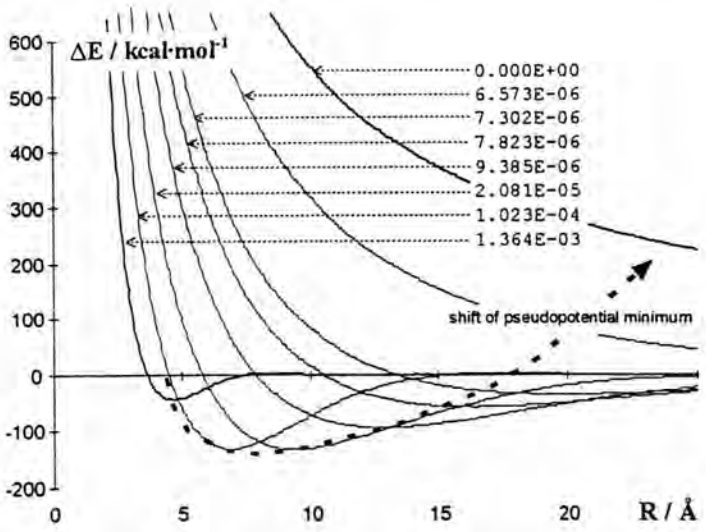

Figure 6.7 Total calcium-calcium interactions at several concentrations of free electrons. The numbers indicate electrons per Å^3, corresponding to 18, 1, 0.2, 0.09, 0.075, 0.07, 0.063, and 0 electrons in 215 ammonia molecules, respectively.

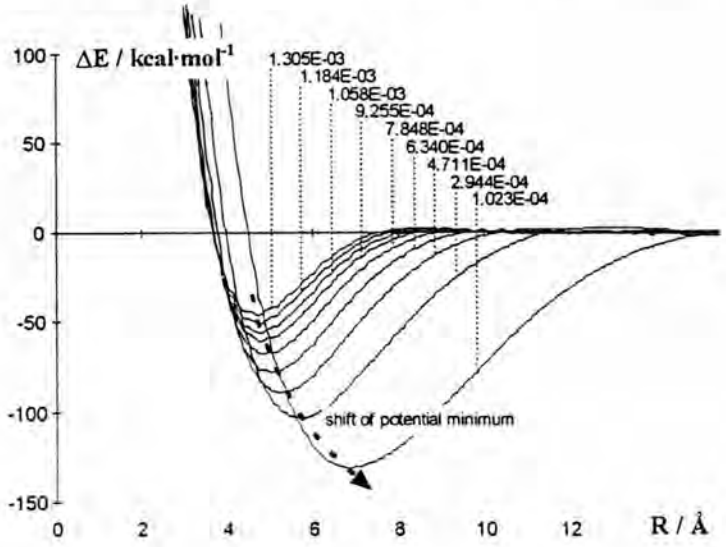

Figure 6.8 Total calcium-calcium interactions at several concentrations of free electrons. The numbers indicate electrons per Å^3, corresponding to 17, 15, 13, 11, 9, 7, 5, 3, and 1 electrons in 215 ammonia molecules, respectively.

Similar investigation have been examined for the total ammonia-ammonia interactions and shown in Figure 6.9, changes of the interactions to that of

pure liquid ammonia when electron concentrations approach zero is clearly demonstrated.

As mention in section 5.4.2, simulations using pseudopotential model I and II have to be carried out with rigid ammonia model to avoid the collapse of ammonia molecules. Snapshot of the two run, after equilibration, are given in Figure 6.9 (a), (b). These plots indicate the failure of the pseudopotentials models I and II. Therefore, detailed information on structure and dynamics properties of the solution have been evaluated only for the simulation using pseudopotential model III, *the point ion model with Gurskii dielectric function*,

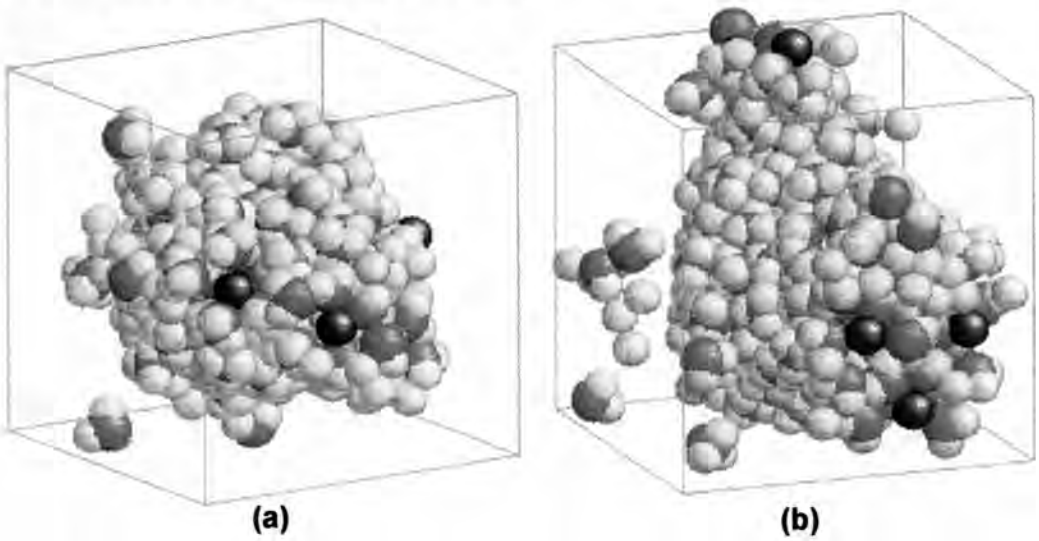

Figure 6.9 System containing 7.725 mole percent of calcium ions in liquid ammonia using the pseudopotential (a) model I (b) model II. The single red balls represent calcium ions. The white balls together with blue balls represent ammonia molecules (white for hydrogen and blue for nitrogen.

Three models of pseudopotentials were tried in this work, but only one of them provided an acceptable result. The other two resulted in the collapse of calcium-ammonia, with all particles in the system forming a spherical ball near the center of the cube. Then ammonia molecules in the simulations were broken up by very strong forces from their neighbors. Only one model, *the point ion model with Gurskii*

dielectric function, can avoid this fate and work for a very long time and come to equilibrium.

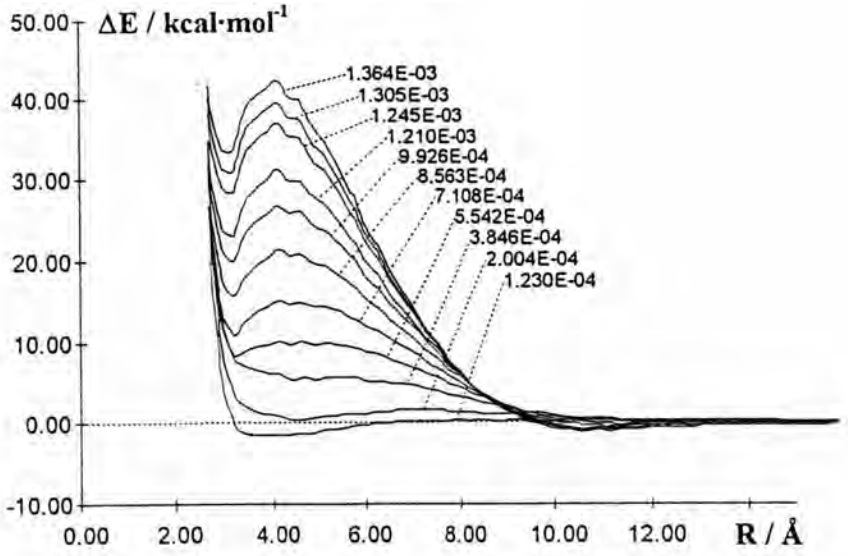

Figure 6.10 Ammonia-ammonia potential at several concentrations of free electrons. The numbers indicate electrons per Å^3, corresponding to 18, 17, 16, 14, 12, 10, 8, 6, 4, 2, and 1 electrons in 215 ammonia molecules, respectively.

6.3 Structural Properties

6.3.1 Solvent structure

To verify the consistency between the simulation model and experimental data, the N-N RDF measured for pure liquid ammonia by X-ray techniques at 277 K [Weast 1976] is compared with that calculated from the simulations with and without three-body corrections (Figure 6.11). The good agreement indicates the reliability of the ammonia model used in this work. The slight shift of the simulated N-N RDF toward the X-ray diffraction data when the three-body correction was taken into account shows that the three-body correction could have an appropriate influence on the structure of the bulk solvent.

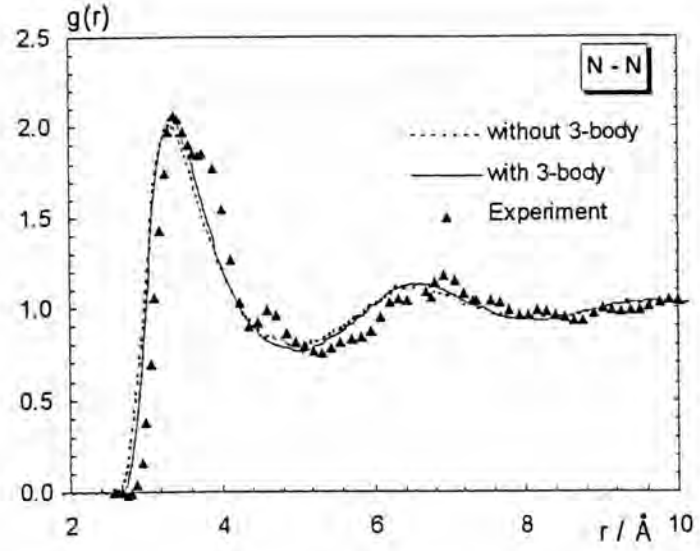

Figure 6.11 Nitrogen-nitrogen radial distribution functions for the dilute Ca(II)-ammonia solution at 240 K. The experimental data at 277 K are from Narten [1977]

To establish the changes in the solvent structure, the nitrogen-nitrogen, nitrogen-hydrogen, and hydrogen-hydrogen RDFs of two different concentrations are compared (Figure 6.12). The N-N RDF of the dilute solution shows a smooth peak that is quite consistent with that of pure ammonia (Figure 6.11). The first shell coordination numbers for dilute and concentrated solutions integrating up to the first minimum of the N-N RDF, are 12 and 8, respectively. The distance to the first minimum in the N-N RDF for the dilute solution indicates the freedom of ammonia molecules to move apart from their neighbors. However, in the concentrated solution, the first peak of the N-N RDF grows rapidly and to a very high peak, while the RDF at the first minimum is close to zero, in contrast to that for the dilute solution. These results suggest that the nearest-neighbor ammonia molecules are tightly clustered together. The second peak and minimum exhibit similar behavior, indicating a well-defined solvation shell in concentrated solutions. The characteristics of the simulated RDFs have been summarized in Table 6.4.

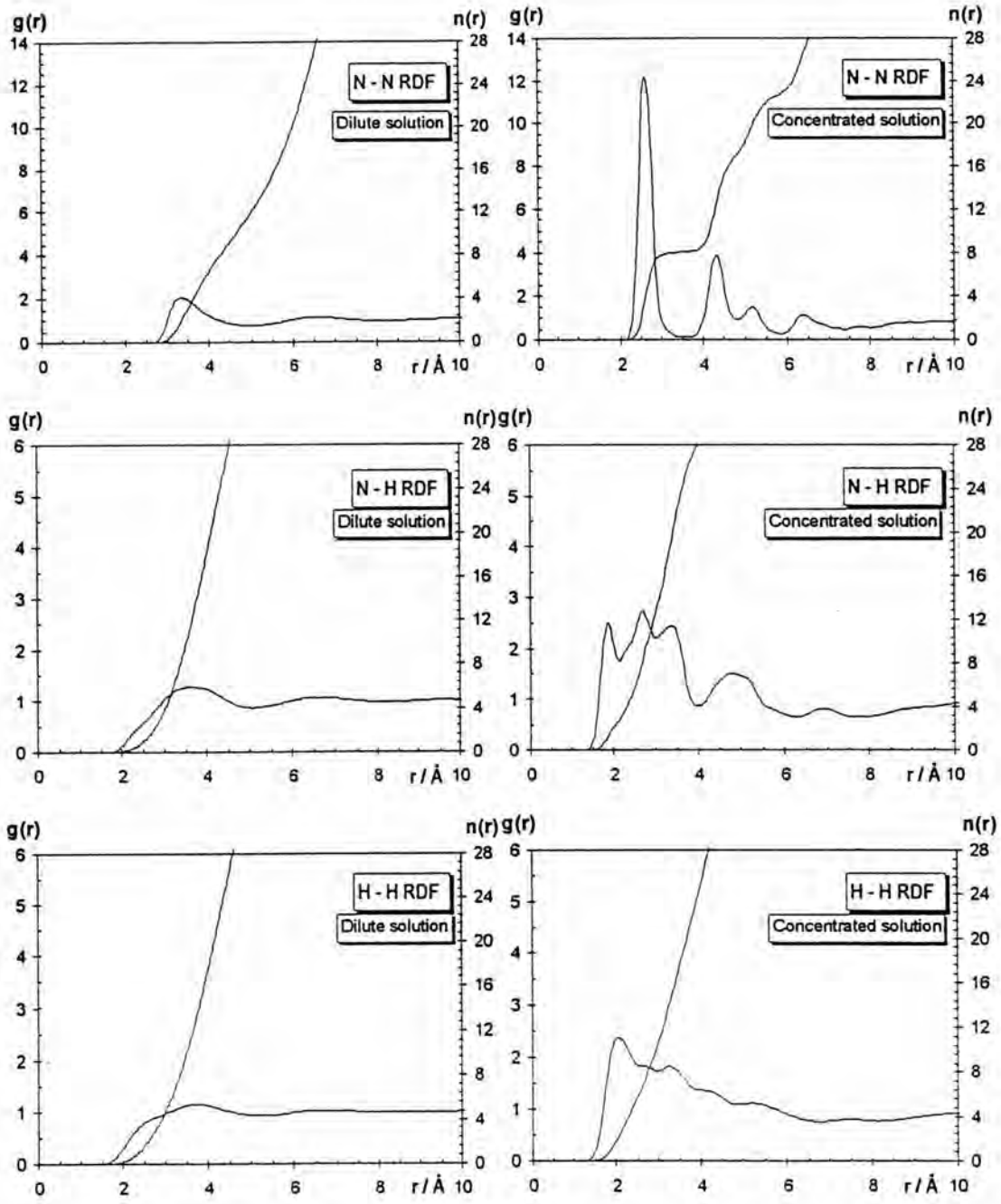

Figure 6.12 Radial distribution functions and running integration numbers for dilute (left) calcium-ammonia solution and concentrated (right) calcium-ammonia solutions.

Attention is centered on the appearance of the well defined peaks of the N-N RDF at 4.2, 5.4 and 6.4 Å. The first shell coordination number of ammonia molecules of 8 suggests a cubic configuration around the central ammonia (Figure 6.13). The related distances between the two ammonia molecules lying on the edges (e.g., N1-N2), on the diagonal lines of the faces (e.g., N1-N3) and on the opposite corners of the cubes (e.g., N1-N7) are 3.1 Å, 4.2 Å, and 5.4 Å, respectively. The later two distances, 4.2 Å and 5.4 Å, lead to the second and the third peaks of the N-N RDFs of high concentrated calcium-ammonia solution shown in Figure 6.12. The disappearance of the N-N RDF at 3.1 Å can be understood from the fact that those ammonia molecules are nearest neighbors of each other', therefore, each nearest pair (e.g. N1-N2 or N1-N4 or N1-N5) tried to rearrange themselves to the optimal N-N distance, i.e., 2.7 Å as exhibited in the N-N RDF plot. Shortening of all nearest pairs of the 8 neighbors on the edges

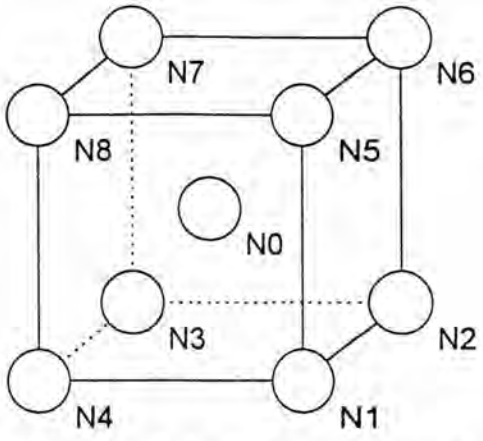

Figure 6.13 Unit cell of the proposed N arrangement.

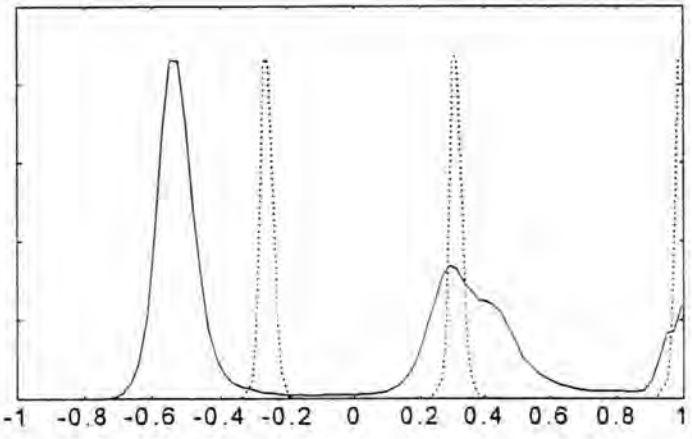

Figure 6.14 Distribution of the N_i-N_o-N_j angles, where N_i and N_j denote two ammonia molecules in the first solvation shell of the central ammonia, N_o, computed from this study (solid line) and from an ideal body-centered cubic configuration (dotted line).

of the cube would lead to a smaller cube and hence a larger stress effect. Therefore, shortening may take place only for the nearest N-N distance of the ammonia molecules in the same group. For example, we can distinguish between a group of ammonia molecules facing lone electron pair of the central ammonia molecule (e.g., one layer in Figure 6.13) and an other facing the hydrogen atoms. Within each group, the nearest N-N distance for the molecules is unchanged. Consequently, the distance between the first N1-N2-N3-N4 layer and the second N5-N6-N7-N8 layer is 3.7 Å, and distance from the first to the third layer above the N5-N6-N7-N8 layer must be 6.2 Å. This corresponds to fourth peak at 6.4 Å of the N-N RDF.

The above conclusion is supported by the distribution plot of the N_i-N_o-N_j angles, where N_i and N_j denote the two ammonia molecules in the first solvation shell of the central ammonia, N_o (Figure 6.14). The ideal cube configuration leads to N_i-N_o-N_j angles of 75.5°, 109.5° and 180° for the two ammonia molecules, i and j, lying on an edge, on the diagonal lines of faces and at the opposite corners of the cubes, respectively. The simulated peaks at 57°, 106° and 180° fit well to the above suggestions, especially when changing the ideal N_i-N_o-N_j angles from 75.5° to 57° for the two molecules lying on the same ages of the cube but not for the others. In addition, broadening of the N_i-N_o-N_j plot is related to the broad distribution of the first shell coordination number of nitrogen atoms (Figure 6.15), in which only a coordination number of 8 corresponds to a cubic structure.

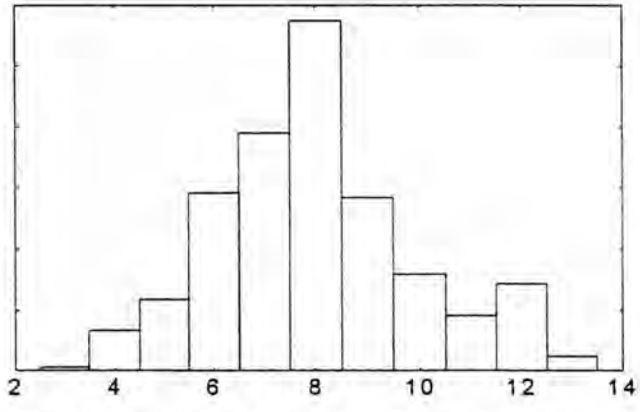

Figure 6.15 Distribution of nitrogen atoms of ammonia molecules around the nitrogen atom of ammonia molecules.

For further investigation of the arrangement of nitrogen atoms, we plotted the distribution of the nitrogen atoms around the ammonia molecules to determine the probability to detect a nitrogen atom in the first solvation shell at an angle δ from the dipole axis of ammonia molecules (Figure 6.16). It shows the preference of ammonia molecules to stay near the nitrogen of another ammonia molecule. In other words, they form clusters with hydrogen atoms pointing to the outside of the cluster.

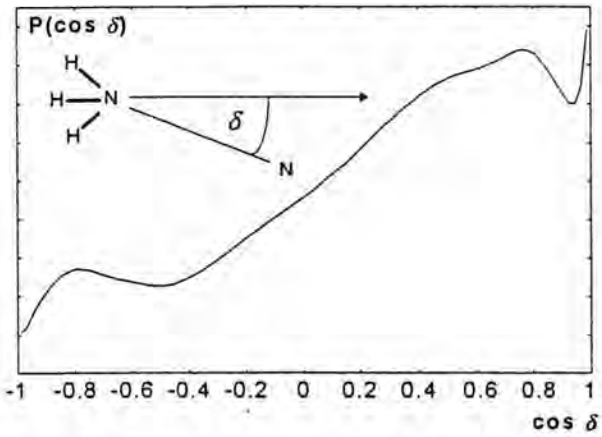

Figure 6.16 Distribution of cos δ for the ammonia molecules in the first solvation shell of an ammonia molecule. The angle δ is defined in the insert.

Although the N-N RDF shows a sharp peak, N-H and H-H RDFs do not, suggesting that the ammonia molecules have orientation freedom. Comparing concentrated and dilute solutions, the distances to the first maximum of N-N, N-H, and H-H RDFs are lower for concentrated solutions (Table 6.4), suggesting that ammonia molecules come closer to their neighbors. We can see that while ammonia molecules gather together, they leave space unoccupied by ammonia to the side. This indicates that there must be some ammonia-free cavities in the concentrated solution. We believe that this space is where the electron density is concentrated (recall that the free electron wave function must be orthogonal to all localized electron states).

Table 6.4 Characteristics of radial distribution functions of Ca(II): R_i, r_{Mi}, and r_{mi} are the distances in Å where for the i-th time $g_{\alpha\beta}(r)$ is unity, maximized, and minimized, respectively, and $n_{\alpha\beta}(r_{m1})$ is the running integration number up to r_{m1}.

	$\alpha\beta$	R_1	r_{M1}	$g_{\alpha\beta}(r_{M1})$	R_2	r_{m1}	$g_{\alpha\beta}(r_{m1})$	r_{M2}	$g_{\alpha\beta}(r_{M2})$	$n_{\alpha\beta}(r_{m1})$
dilute solution without 3-body corrections	N N	2.97	3.30	2.0	4.22	5.07	0.8	6.52	1.1	12.6
	N H	2.94	3.64	1.2	4.44	5.12	0.9	6.53	1.1	39.1
	H H	3.10	3.69	1.1	4.51	5.21	0.9	6.68	1.0	41.1
	Ca N	2.28	2.53	15.1	2.88	3.25	0.2	4.75	2.1	8.97
	Ca H	2.79	3.10	6.8	3.47	3.85	0.2	5.25	1.6	27.4
dilute solution with 3-body corrections	N N	2.99	3.34	2.1	4.25	5.13	0.7	6.60	1.1	12.8
	N H	2.97	3.67	1.2	4.49	5.02	0.9	6.69	1.1	36.8
	H H	3.08	3.81	1.1	4.55	5.37	0.9	6.73	1.0	44.8
	Ca N	2.51	2.86	5.1	3.30	3.98	0.3	5.28	1.5	8.19
	Ca H	3.08	3.39	3.4	3.81	4.42	0.4	5.68	1.2	24.3
concentrated solution	N N	2.29	2.60	3.6	2.98	3.65	0.1	4.31	3.8	8.09
	N H	1.65	2.69	2.7	3.83	4.00	0.9	4.80	1.5	28.15
	H H	1.69	2.07	2.4	-	2.95	1.7	-	-	9.96
	Ca N	4.65	5.19	1.4	-	-	-	-	-	-
	Ca H	4.35	6.86	1.4	-	-	-	-	-	-
	Ca Ca	3.48	3.92	10.3	4.84	5.41	0.5	6.00	1.1	2.35

To investigate the phenomenon more directly, "snapshots" were taken at certain times. All snapshots clearly show that ammonia molecules gather into clusters, and the calcium ions are floating in the cavities.

For example, in Figure 6.17, the ammonia clusters are spirals, and the cavities and clusters wind around each other. In other snapshots, cavities appear to be tunnels through ammonia filled regions, or vice versa. We can see the hydrogen atoms at the surface of ammonia clusters, as expected. Unfortunately, the size of the system is too small for us to examine the topology of cavities and clusters in more detail. From the high observed conductivity it is expected that the cavities should be globally interconnected. We hypothesize that the free electrons penetrate the cavities, because the free electron wave functions have zero overlap with core electron wave functions. Also, simulations by Deng, Martyna, and Klein [1992, 1994] demonstrated this behavior, with free electrons throughout the cavities (Figure 6.18).

In the present simulations, calcium ions were found exclusively in the cavities, i.e., where it is believed the free electrons reside. This is different from the result for lithium ions in liquid ammonia [Hannongbua et al. 1997] and for cesium in

ammonia [Deng et al. 1994], demonstrating that lithium ions and cesium ions avoided the cavities and were only found in ammonia clusters (Figure 6.18).

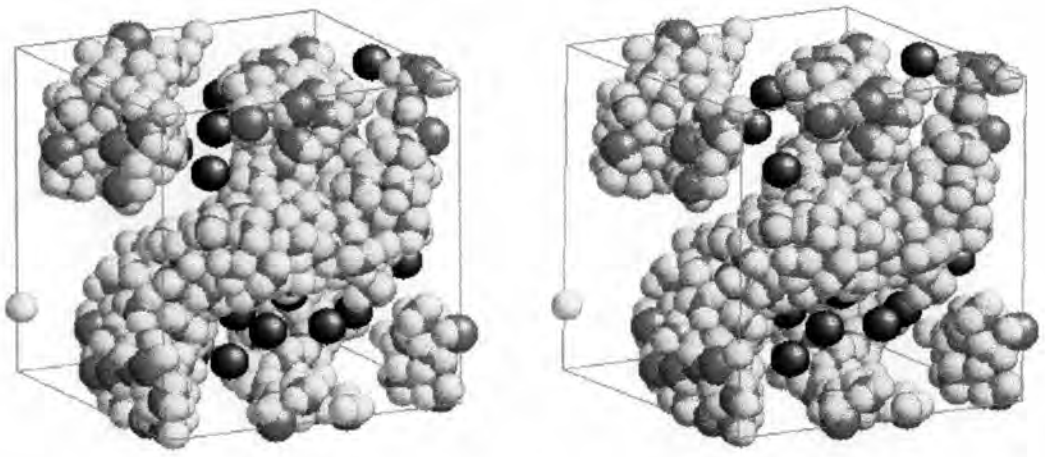

Figure 6.17 Stereogram of the simulation system. It can be seen that the system is not homogenous. There are cavities in between the clusters of ammonia molecules. The single red balls represent calcium ions. The white balls together with blue balls represent ammonia molecules (white for hydrogen and blue for nitrogen).

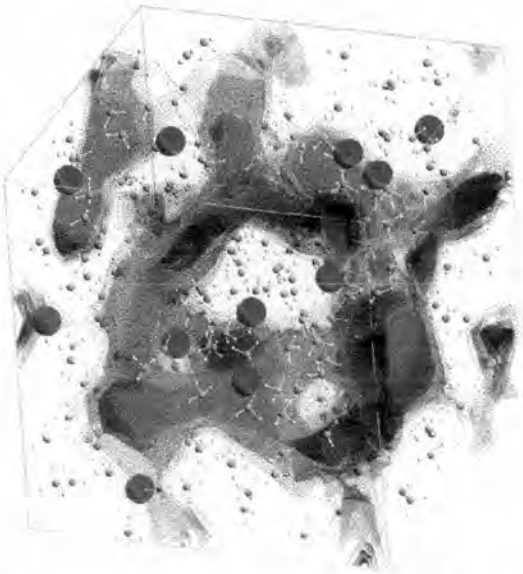

Figure 6.18 The electron density of a representative configuration of a cesium-ammonia solution at high electron concentration. The system consists of 24 cesium ions (purple balls) in 256 ammonia molecules [Klein 1994].

6.3.2 Ion-solvent structure

6.3.2.1 Dilute solution

Another interesting property one can study from the simulation results is the solvation shell structure that can be established by plotting RDFs of the species pairs involved in the solution. The Ca(II)-N and Ca(II)-H radial distribution functions, and also their corresponding integration numbers obtained from simulations, are compared in Figure 6.19.

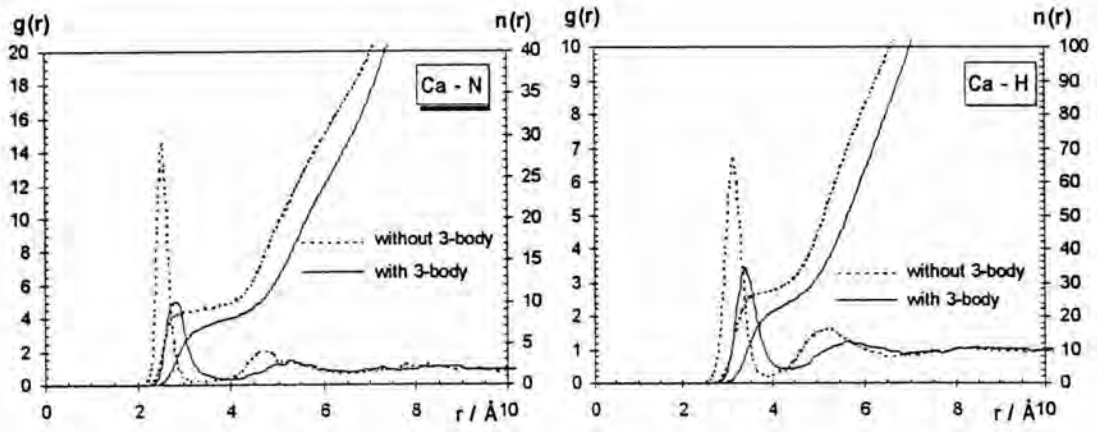

Figure 6.19 Ca(II)-N and Ca(II)-H radial distribution functions and corresponding running integration numbers for simulations without (dotted line) and with (solid line) three-body corrections of the dilute calcium-ammonia solution.

Without the three-body correction, the Ca(II)-N RDF shows the first sharp peak centered at 2.53 Å. The integration number up to the first minimum of 3.25 Å is 9. With the three-body correction, the first peak shifts to 2.86 Å, the first minimum is at 3.98 Å and the first shell coordination number reduces to 8. It is interesting to note that shift of the first peak position by 0.33 Å in this study is much higher than increase by 0.12 Å for Mg(II) [Hannongbua 1997] and decreases by 0.08 Å for Zn(II) [Hannongbua et al. 1992] in liquid ammonia. The significant increase of the size of the first solvation shell for Ca(II) can be understood in terms of the loose binding of the solvent molecules into a bigger solvation sphere for Ca(II) (r_{op}=2.41 Å

and the corresponding stabilization energy, ΔE_{op}=-62.6 kcal.mol^{-1}) as compared with Mg(II) (r_{op}=2.06 Å, ΔE_{op}=-95.7 kcal.mol^{-1}) and Zn(II) (r_{op}=1.95 Å, ΔE_{op}=-94.1 kcal.mol^{-1}) [ibid]. On the other hand, it was found that the calculated size of the first solvation sphere for singly charged Li(I) and Na(I) in liquid ammonia remains unchanged when the three-body corrections are applied [ibid].

The influence of the three-body corrections on the second peak of the Ca(II)-N RDF is also different from that on the other doubly charged ions, Mg(II) and Zn(II). As a consequence of the loosely bound solvation sphere of Ca(II), the three-body effect causes the disappearance of a well-recognized second peak of the Ca(II)-N RDF while this effect for Mg(II) and Zn(II) leads to a slight shift of the second peak to longer distances.

The Ca(II)-H RDFs of simulations with and without three-body corrections show a sharp first peak at 3.39 Å and 3.10 Å containing 27 and 24 hydrogen atoms, respectively. Changes due to the three-body corrections are similar to those for the Ca(II)-N RDF. As expected, no significant difference has been detected between the N-N, N-H, and H-H RDFs of the two runs. Their characteristics as well as those of the Ca(II)-N and Ca(II)-H RDFs have been summarized in Table 6.4.

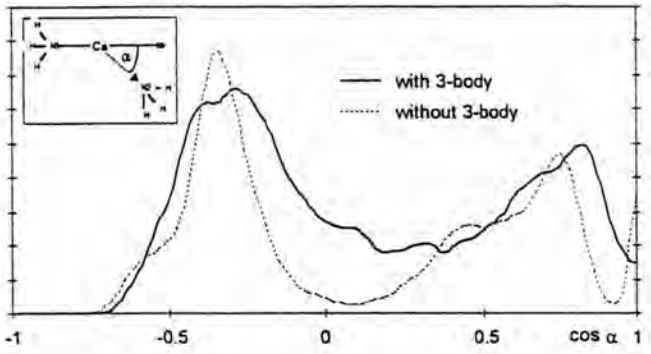

Figure 6.20 Distribution of the cosine of the N-Ca(II)-N angle, p(cos α), for pairs of ammonia molecules in the first solvation sphere of the dilute calcium-ammonia solution. The angle α is defined as in the insert.

To monitor the short-range structure of the 9 (or 8) ammonia molecules in the first solvation shell for simulations without (or with) three-body corrections, we examine the configuration-averaged distribution of the N-Ca-N angle for pairs of solvent molecules in the first shell (Figure 6.20).

Note that the optimal spacing of 8 solvent molecules equidistant from the solute would give rise to a cubic configuration. With respect to a given solvent molecule, 3 other molecules would be at an N-Ca(II)-N angle of 70.5°, another 3 at 109.5°, and 1 at 180°; the cosines of these angles are 1/3, -1/3, and -1, respectively. The simulation results without three-body corrections show a sharp peak centered close to 1/3 and a large gap between that peak and a further peak ($\cos\alpha \approx 1/3$), indicating a cubic structure that is distorted to accommodate a ninth molecule. When three-body corrections are included, the distribution is qualitatively similar, but the peaks are much broader, indicating that the expected structure of the 8 ammonia molecules in the first solvation shell is a less rigid, time-varying, distorted cubic configuration.

Figure 6.21 shows the distribution of $\cos\beta$ which is defined as the angle between the vector pointing from the calcium ion to the nitrogen atom and the dipole vector for an ammonia molecule located in the first solvation shell. The distributions obtained from both simulations are sharply peaked at $\cos\beta = 1.0$, with no significant difference between them. The distribution for Ca(II) is broader than that for Mg(II) and narrower relative to that of Na(I) [Hannongbua 1997]. This can be understood in terms of the strength of the interaction energy, $-\mu E\cos\beta$, between the ammonia dipole moment, μ, and the ion's electric field, $E \propto q/r^2$. Based on our simulations, the strength of the electric field at the first solvation shell is ordered by Mg(II) > Ca(II) > Na(I): this explains why Mg(II) has the narrowest $\cos\beta$ distribution and Na(I) has the broadest.

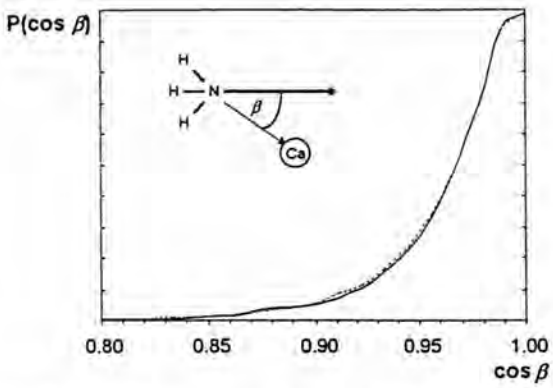

Figure 6.21 Distribution of cos β for ammonia molecules in the first solvation shell of calcium ion (dilute solutions).

6.3.2.2 Concentrated solution

In the concentrated solution, we found all the calcium ions separated from the ammonia groups (Figure 6.22), and floating in the cavities of the solution. This behavior is consistent with the wide distance minima of the calcium-ammonia potential from 2.8 - 7.0 Å (Figure 6.5) as well as the Ca(II)-N RDF from 4.0-10.0 Å which suggests that calcium ions can move without restraint in this region. The Ca(II)-N and Ca(II)-H RDFs show also that no ammonia molecules come closer to a calcium ion than 3.0 Å. In addition, the onset of the Ca(II)-H RDF at about 1 Å before that of the Ca(II)-N RDF indicates that ammonia molecules lay at the surface of the tunnels, pointing H-atoms into the cavities.

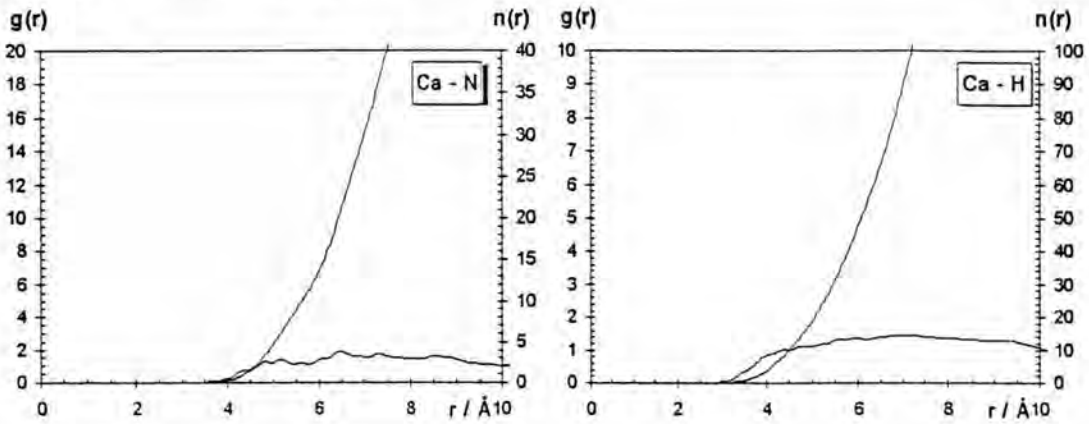

Figure 6.22 Ca(II)-N and Ca(II)-H radial distribution functions and corresponding running integration numbers for concentrated solution simulations.

6.3.3 Ions structure

In the simulations of the high ion concentration solution, with 18 calcium ions in 215 ammonia molecules, the Ca(II)-Ca(II) RDF has been evaluated and plotted in Figure 6.23. A sharp first peak and a well-defined minimum are the consequences of V_{total} describing the calcium-calcium interaction (Figure 6.4). The running integration number up to the first minimum of the RDF of 2.35 (see Table 6.4) includes coordination numbers of 0, 1, 2, 3, 4, 5, and 6 with the percentages of 16%, 28%, 15%, 13%, 15%, 5%, and 3% , respectively.

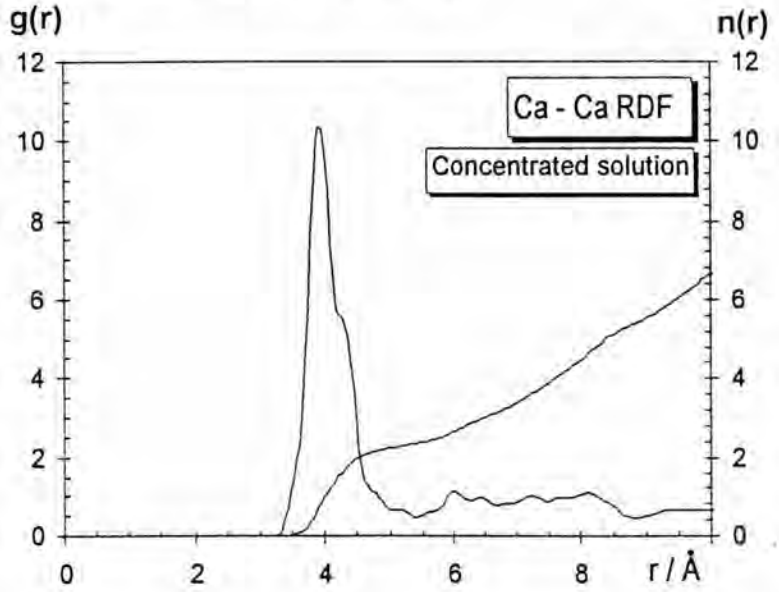

Figure 6.23 Calcium-calcium radial distribution function and running integration number for concentrated solutions simulations.

To investigate the arrangement of the ions in more detail, the distribution of the Ca(II)-Ca(II)-Ca(II) angle was computed and plotted in Figure 6.24. The figure shows two peaks at 180° and 130° covering cos β from -1.00 to -0.85 and from -0.70 to -0.50, respectively. These data and the average coordination number of about two indicate a preferential linking of the calcium ions to linear and bent chains. Some "snapshots" corroborate this interpretation; Figure 6.25 shows an occasion on which several calcium ions were arranged as a long chain. In other snapshots, it is seen

that a cavity is wider so that the calcium ions form other lattice shapes, though their spacing is nearly always close to 4 Å. In either case, the constant spacing of calcium ions in regions with free electrons indicates metallic bonding, the dimensionality of which is less than three.

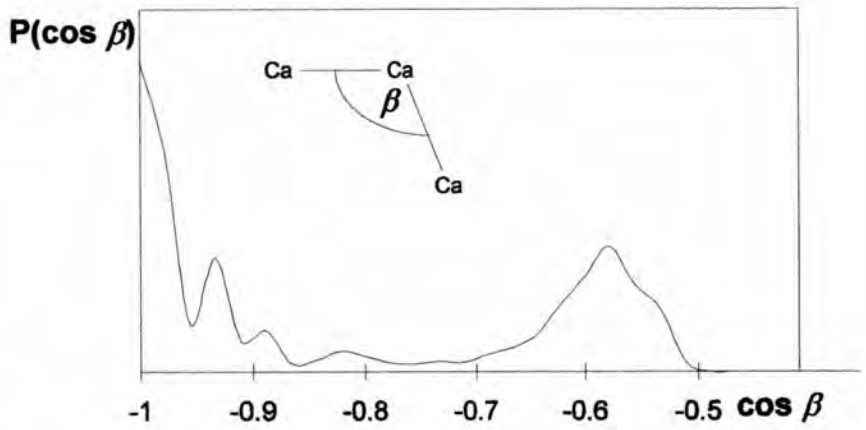

Figure 6.24 Distribution of the cosine of the Ca(II)-Ca(II)-Ca(II) angle, p(cos β), for neighboring calcium ions. The angle β is defined as in the insert.

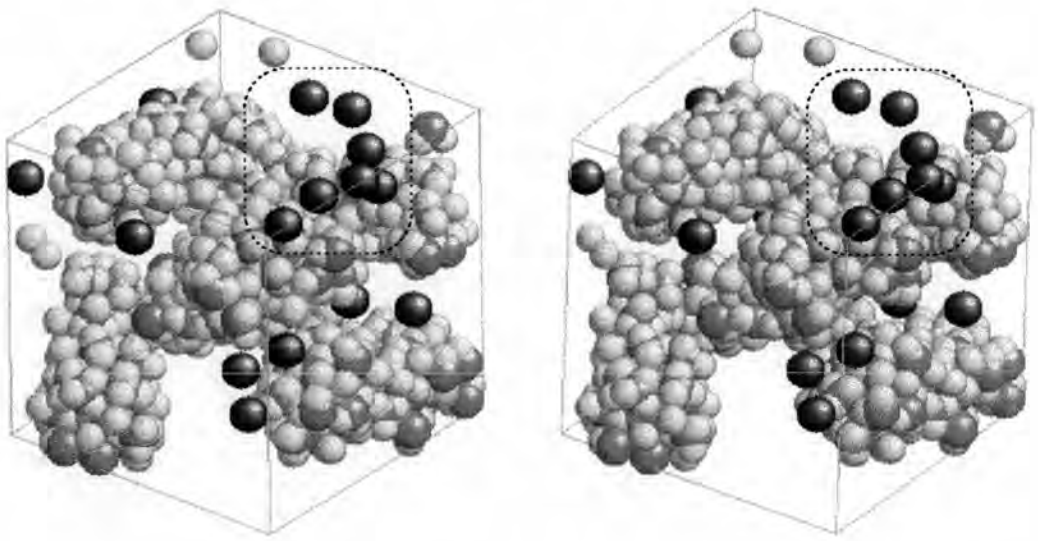

Figure 6.25 Snapshot of the simulation cube where a chain of calcium ions is observed (inside dashed curve). The red balls represent the calcium ions. The white balls and blue balls represent hydrogen and nitrogen atoms, respectively, of ammonia molecules.

6.3.4 Intermolecular and intramolecular structure of the solvent

6.3.4.1 Dilute solution with and without three-body corrections

A benefit of the flexible model for the ammonia molecule is that it allows one to investigate changes of the molecular geometry. In Figure 6.26, distributions of the N-H and H-H distances and H-N-H angle of ammonia molecules in the first solvation shell of the dilute solution are shown.

The figure indicates a slight decrease in the average N-H bond length, where the three-body corrections are applied. In all three plots three-body corrections lead to a sharpening of all peaks which implies a weaker binding of the ammonia molecules in the first solvation shell of Ca(II). Conversely, there are no significant changes in the molecular geometry for bulk ammonia. Therefore the calculated results are not displayed.

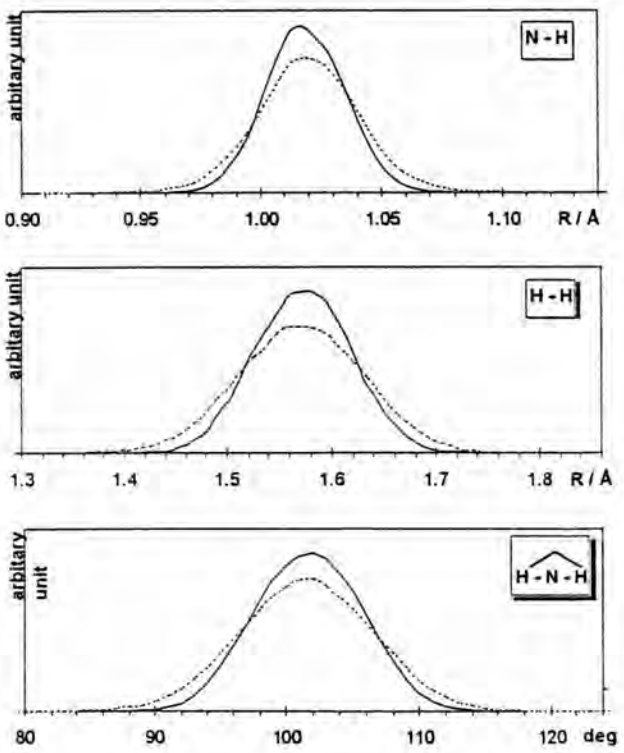

Figure 6.26 Normalized distributions of the intramolecular distances and angles of ammonia molecules in the first solvation shell of the dilute solution with (solid lines) and without (dashed line) three-body corrections.

6.3.4.2 Dilute and concentrated solutions

In Figure 6.27, the distributions of the N-H and H-H distances and the H-N-H angle of ammonia molecules in the bulk are shown for diluted and concentrated solutions.

In the concentrated solution, there were no ammonia molecules in the solvation shell of a calcium ion because the ions were in the ammonia free cavities. A significant decrease due to the pseudopotential was found for all plots, suggesting that ammonia molecules in the concentrated solution are under more stress due to the cluster formation.

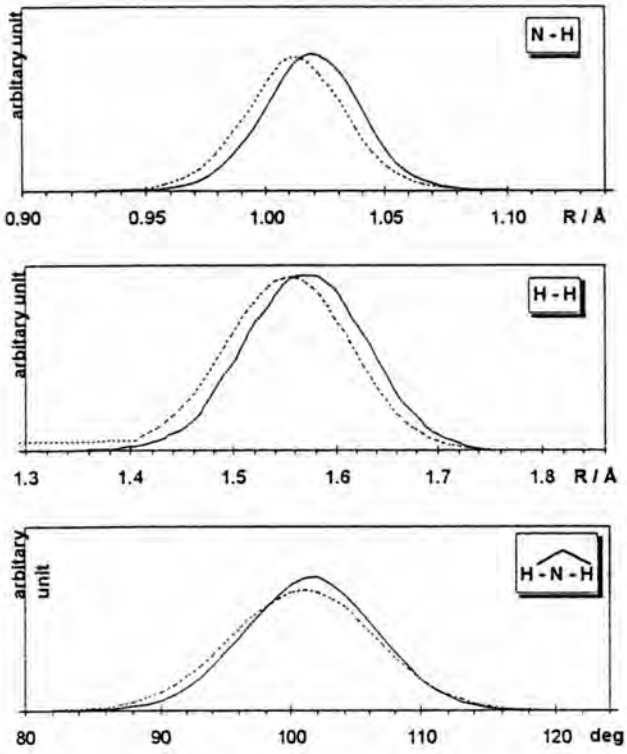

Figure 6.27 Normalized distributions of the intramolecular distances and angles of ammonia molecules in the bulk for the dilute solution (solid lines) and concentrated (dashed) solutions.

6.4 Dynamical Properties

6.4.1 Translationtional motions

6.4.1.1 Dilute solution

Translational motions of the molecules can be represented by the velocity autocorrelation function (VACF). The center-of-mass VACFs of the two simulations, with and without the three-body corrections, both for molecules in the bulk and the first solvation shell have been calculated separately and plotted in Figure 6.28. The spectral density, $\Im(\omega) = \int_0^\infty C_v(t)\cos(\omega t)\,dt$, obtained from the VACF, $C_v(t)$, is plotted in Figure 6.25.

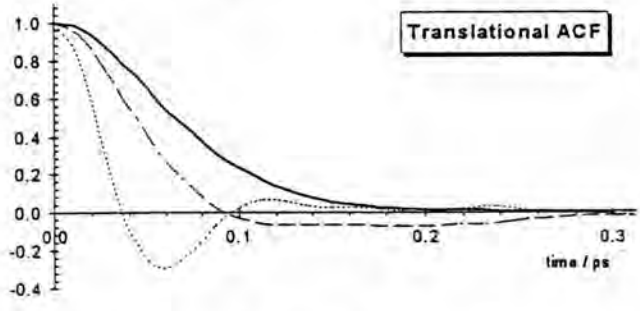

Figure 6.28 Normalized center of mass velocity autocorrelation functions for ammonia molecules in the bulk (solid line) and in the first solvation shell of Ca(II) obtained from the simulations with (dashed line) and without (dotted line) three-body corrections for the system consisting of 1 calcium ions in 215 ammonia molecules.

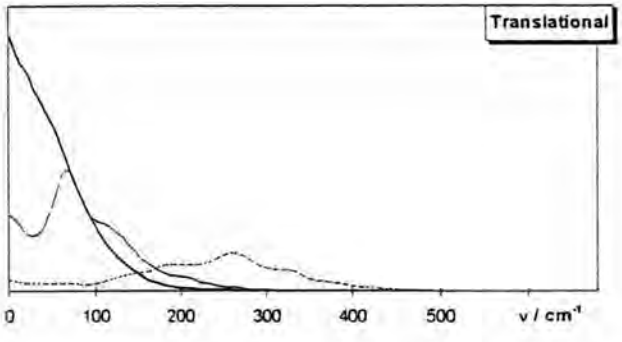

Figure 6.29 Spectral density of the translational motions of the normalized center of mass velocity autocorrelation functions shown in Figure 6.28 for ammonia molecules in the bulk (solid line) and in the first solvation shell of Ca(II) obtained from the simulations with (dashed line) and without (dotted line) three-body corrections for the system consisting of 1 calcium ions in 215 ammonia molecules.

The VACFs for bulk molecules decay smoothly to zero at about 0.25 ps for both runs. The VACF for molecules in the first solvation shell for the simulation using only the pair potentials crosses zero at 0.038 ps before overshooting due to a restoring force, which is much faster than the time of 0.086 ps when the three-body effects are included. The spectral densities of the three types of molecules (bulk, first solvation shell with three-body corrections, and first solvation shell using only pair potentials), peak at 0, 67, and 259 cm^{-1}, respectively (Figure 6.29). As expected, bulk molecules can translate freely (with zero frequency) while solvated molecules are bound more tightly when the three-body corrections are neglected. In conclusion, the VACF and spectral density plots indicate that the three-body corrections yield looser binding of the solvated molecules.

It is found experimentally that the self-diffusion coefficient (D) of liquid ammonia is strongly temperature dependent [Garroway and Cotts 1973], and it is not yet possible to model that properly using simulation data [Impey and Klein 1984]. A self-diffusion coefficient for bulk ammonia calculated in our previous work [Hannongbua et al. 1988] using the same NH_3-NH_3 pair potential as in this study, and calculated by Garroway et al. [1973] are approximately 70% too high and 80% too low, respectively, compared with the experimental value at 277 K of 5.3×10^{-5} cm^2s^{-1} [O'Reilly, Peterson, and Scheie 1973]. However, for the ammonia molecules in the first solvation shell of Ca(II) we obtained $D = (3.80\pm2.22)\times10^{-4}$ cm^2s^{-1} and $D = (5.75\pm 2.35)\times10^{-5}$ cm^2s^{-1} for the simulations with and without three-body corrections, respectively. The relatively large error is due to the fact that there are only a few ammonia molecules involved in the statistical calculations.

6.4.1.2 Concentrated solution

Figure 6.30, the VACF for the concentrated solution crosses zero at about 0.018 ps before bouncing back due to a restoring force. This value is much

smaller than those of ammonia molecules in the solvation shell of calcium ions and in the bulk of the dilute solution. The spectral density of the concentrated solutions (Figure 6.31) shows broad peaks at 517 cm^{-1}, indicating a tighter binding of the ammonia molecules in the concentrated solution than in the dilute solution. The diffusion coefficient for the dilute and concentrated solutions are (1.24±0.19)x10^{-4} cm^2s^{-1} and (7.08±0.16)x10^{-6} cm^2s^{-1}, respectively. From equation (3.20), $D=(1/6\pi a)(k_BT/\nu)$, and the van der Waals radius of ammonia of 1.54 Å [Hodgman 1959], the viscosity of the solution can be evaluated. The calculated values at 233 K of 0.092 $gm\cdot cm^{-1}\cdot s^{-1}$ for the dilute solution and of 1.612 $gm\cdot cm^{-1}\cdot s^{-1}$ for the concentrated solution are plotted in Figure 6.33 along with those measured experimentally [Thompson 1976]. A qualitative agreement between the simulated and the experimental viscosities indicates reliability of the diffusion coefficients obtained from the concentrated solution simulations.

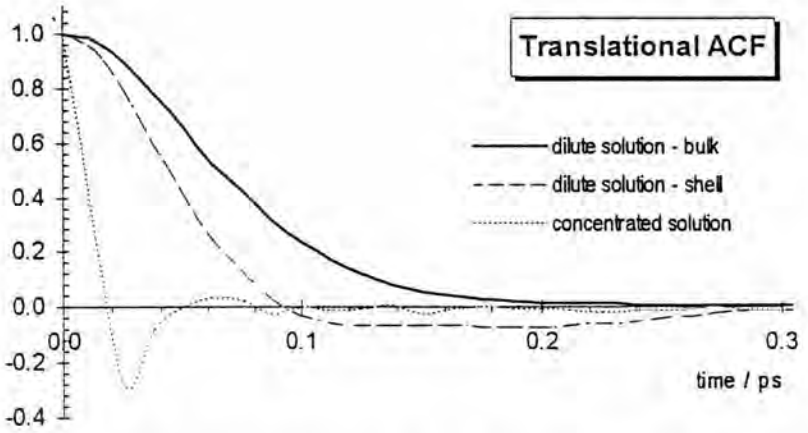

Figure 6.30 The VACFs for ammonia molecules in the bulk and first solvation shell of Ca(II) obtained from the simulations with three-body corrections for the dilute (1 Ca(II) in 215 NH_3), and concentrated solution (18 Ca(II) in 215 NH_3).

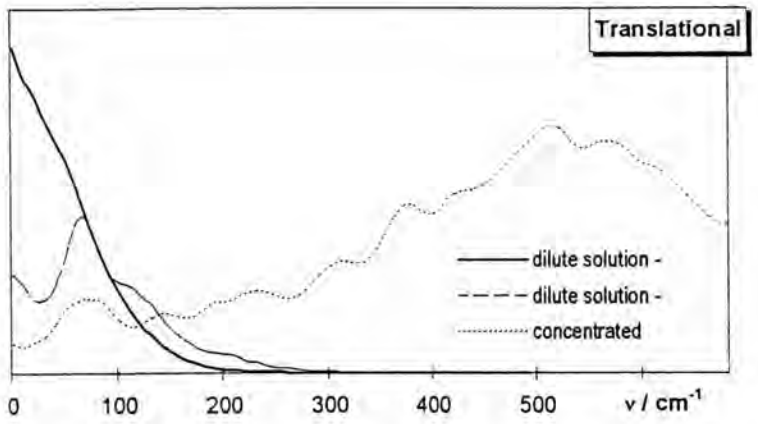

Figure 6.31 The Fourier transforms of VACFs, shown in Figure 6.27, for ammonia molecules in the bulk and first solvation shell of Ca(II) obtained from the simulations with three-body corrections for the dilute (1 Ca(II) in 215 NH_3), and concentrated solution (18 Ca(II) in 215 NH_3).

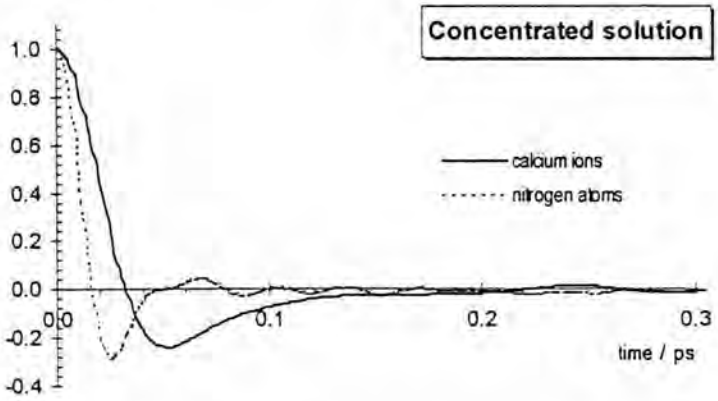

Figure 6.32 The VACFs for calcium ions and nitrogen atoms obtained from the simulations with three-body corrections for the concentrated solution (18 Ca(II) in 215 NH_3).

The VACFs of calcium ions in the concentrated solution are shown in Figure 6.32. The plot for calcium ions approach zero at 0.032 picosecond. The simulated diffusion coefficient for the calcium ions in this solution is $(1.08\pm0.16)\times10^{-5}$ cm^2s^{-1}. Since the calcium ions have smaller size than the ammonia, relation (3.20) predicts that the diffusion coefficient of calcium ions should be greater than for ammonia molecules. As it was expected, the simulations give the result $D = (7.08\pm 1.12)\times10^{-6}$ for ammonia molecules and $D = (1.08\pm0.16)\times10^{-5}$ for calcium ions. These indicate that calcium ions can move with more loosely in solution in the simulation, coincide with discussion in section 6.3.1.

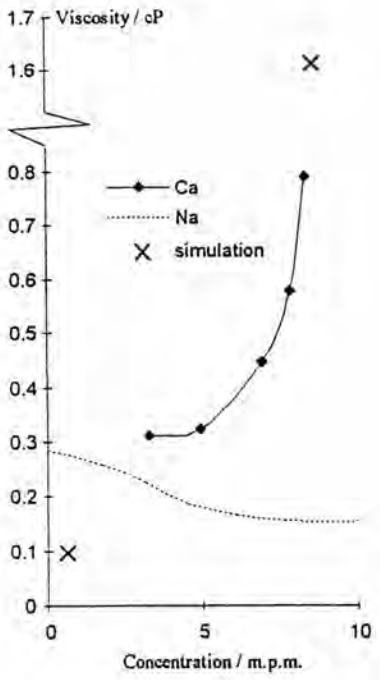

Figure 6.33 Calculated (240 K) and experimental (233 K) viscosity of calcium-ammonia and sodium-ammonia solutions[Thompson 1976].

6.4.2 Librational motions

Librational dynamics of the ammonia molecules in the simulated system can be studied through the Fourier transform of the ACFs of velocity components of hydrogen atoms. Details of the projections of the velocities onto degenerate axes are explained by Bopp [1986].

The spectral densities of the librational motions of ammonia in the bulk and in the solvation shell of dilute solutions are presented in Figure 6.34. For rotation about the x-axis (the coordinate system is shown in Figure 5.1), the frequency increases from about 200 cm^{-1} in the bulk to about 400 - 600 cm^{-1} in the solvation shell of the Ca(II) with and without three-body corrections. The corresponding peak for the concentrated solutions appear at 500 cm^{-1}, with a broad distribution as shown in Figure 6.35.

For z-axis free rotation at zero frequency were found for dilute solution while that of concentrated solution speak at about 230 cm^{-1} covered from zero to about 600 cm^{-1} (Figures 6.36 and 6.37).

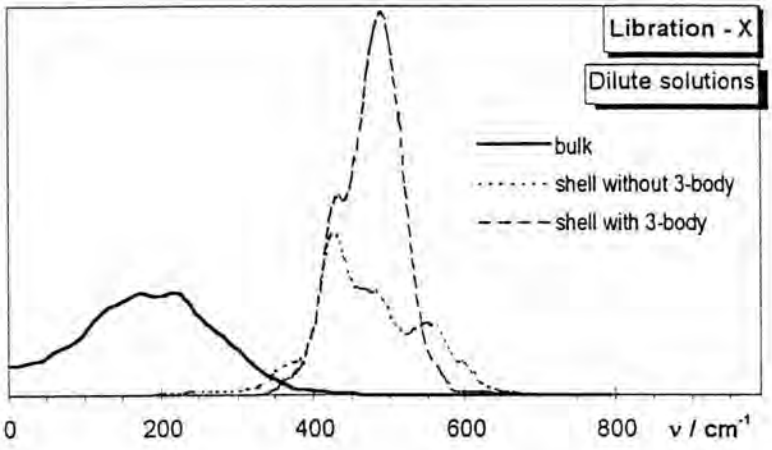

Figure 6.34 Spectral density of the rotation about x-axis (defined by the configuration of the first ammonia molecule in Figure 5.2) for ammonia molecules in the bulk and the first solvation shell of Ca(II) obtained from our the simulations with and without three-body corrections.

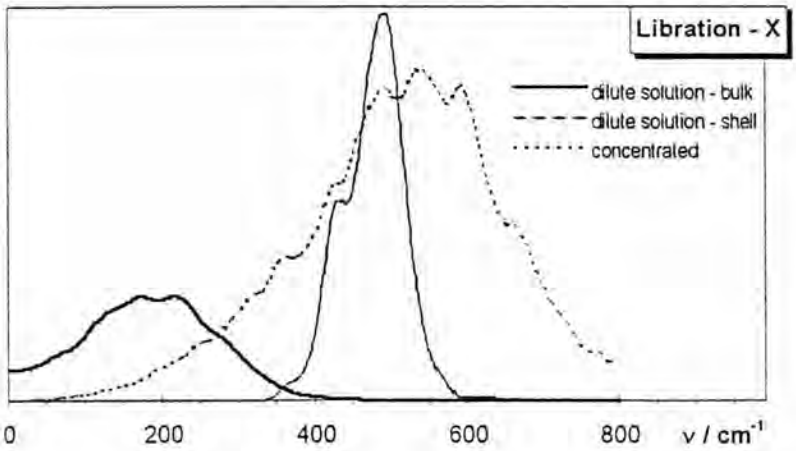

Figure 6.35 Spectral density of the rotation about x-axis for ammonia molecules in the bulk and the first solvation shell of Ca(II) obtained from the simulations of dilute solutions, and in the bulk of concentrated solutions.

The difference between rotational frequency about x- or y-axis of the bulk and solvated molecule in dilute solution can be easily understood on the basis of the structure of the solution. The solvation forces keep the dipole vector of the

solvated molecules antiparallel to the N-Ca(II) vector. Thus the Ca(II)-ammonia interactions hinder the motion around the x- and y-axes but not the rotation around the dipole axis.

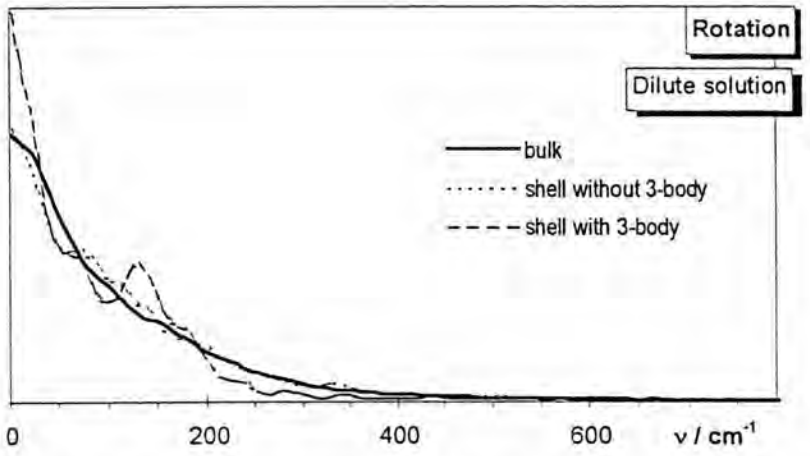

Figure 6.36 Spectral density of the rotational motion about the z-axis (dipole moment) for the molecules as defined in Figure 5.1.

Shift of all rotational modes to higher frequencies form the concentrated system relative to the dilute one is due to a cluster formation of the ammonia molecules. Broaden of all peak is also the consequence of this fact.

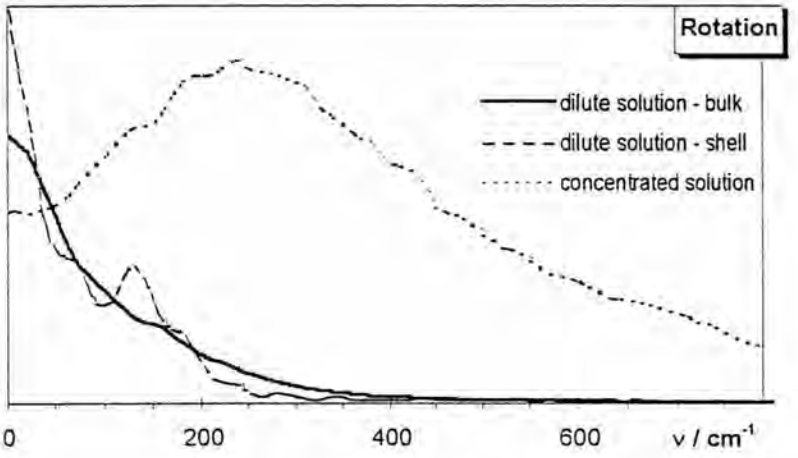

Figure 6.37 Spectral density of the rotational motion about the z-axis (dipole moment) for the molecules as defined in Figure 5.1. Comparison between the dilute solution with the concentrated solution.

6.4.3 Vibrational motions

Various modes of vibrational frequencies calculated from the simulations of dilute and concentrated solutions are compared in Table 6.5, as well as those obtained experimentally. Note that statistical uncertainties in the calculation frequencies are approximately ±20 cm^{-1}. The symmetric stretching and asymmetric bending modes are blueshifted in the solvation shell of the dilute solution by 167 cm^{-1} and 83 cm^{-1}, respectively, while the symmetric bending shows a redshift of 126 cm^{-1}. However, there is no significant change for asymmetric stretching in the dilute solution. In the bulk of the concentrated solution, compare with that of the dilute one, all modes of vibrations are blueshifted. The symmetric bending, asymmetric bending, symmetric stretching, and asymmetric stretching modes are shifted by 76 cm^{-1}, 38 cm^{-1}, 116 cm^{-1}, and 74 cm^{-1}, respectively. In both simulations and experiment all symmetric modes are found at lower frequencies than the corresponding asymmetric ones.

The vibrational frequencies from experiments and from simulations are consistent. Qualitative agreement of the vibrational frequency of the bulk molecules indicates the quality of the potential used. The blueshift of the symmetric bending and redshift of the symmetric stretching modes for the molecules in the solvation shell indicate the influence of the calcium ion on the ammonia molecules. Similar effects were also found in the system of Li(I) in liquid ammonia [Hannongbua 1988] and K(I) and I(-) in liquid ammonia [Tongraar et al. 1997]. The effect of adding three-body corrections on these frequencies were not strong, except for a slightly decreasing shift in the anti-symmetric stretching mode, as shown in Figure 6.38.

Table 6.5 Frequencies response from experiments and from simulations of liquid ammonia

Mode	Ca(II)-NH_3 simulations			pure ammonia experiment data	
	dilute solution solvation shell	dilute solution bulk liquid	concentrated solution	liquid†	gas‡
Sym. Bend.	1310	1184	1386	1066	932, 968
Asym. Bend.	1560	1643	1598	1638	1627
Sym. Stretch.	3251	3418	3367	3240	3336
Asym. Stretch.	3557	3580	3631	3379	3444

†[Birchall and Drummond 1970] ‡[Spirko 1983].

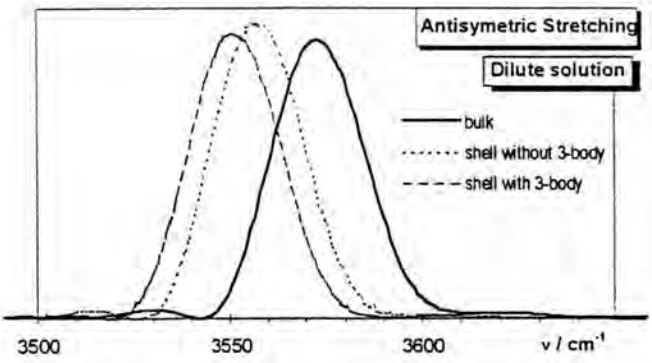

Figure 6.38 Spectral density of the anti-symmetric stretching for the ammonia molecules in dilute solution.

In the contrast case, ammonia molecules in concentrated solution are strongly influenced by their neighbor. In Figure 6.39, broaden of the anti-symmetric stretching indicate that molecules are undergoing various sorts of interactions.

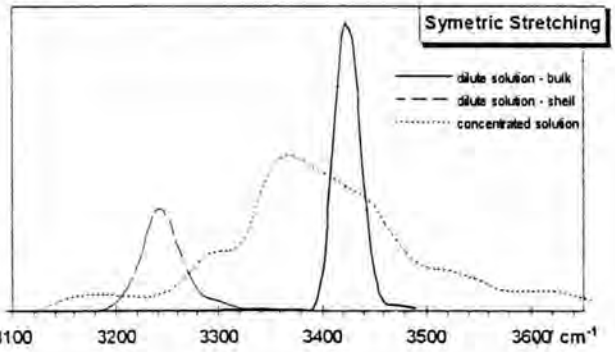

Figure 6.39 Comparison of anti-symmetric stretching spectrum for the ammonia molecules in the bulk and the first solvation shell of Ca(II) in dilute solution obtained from the simulations with three-body corrections, and in bulk of concentrated solution.

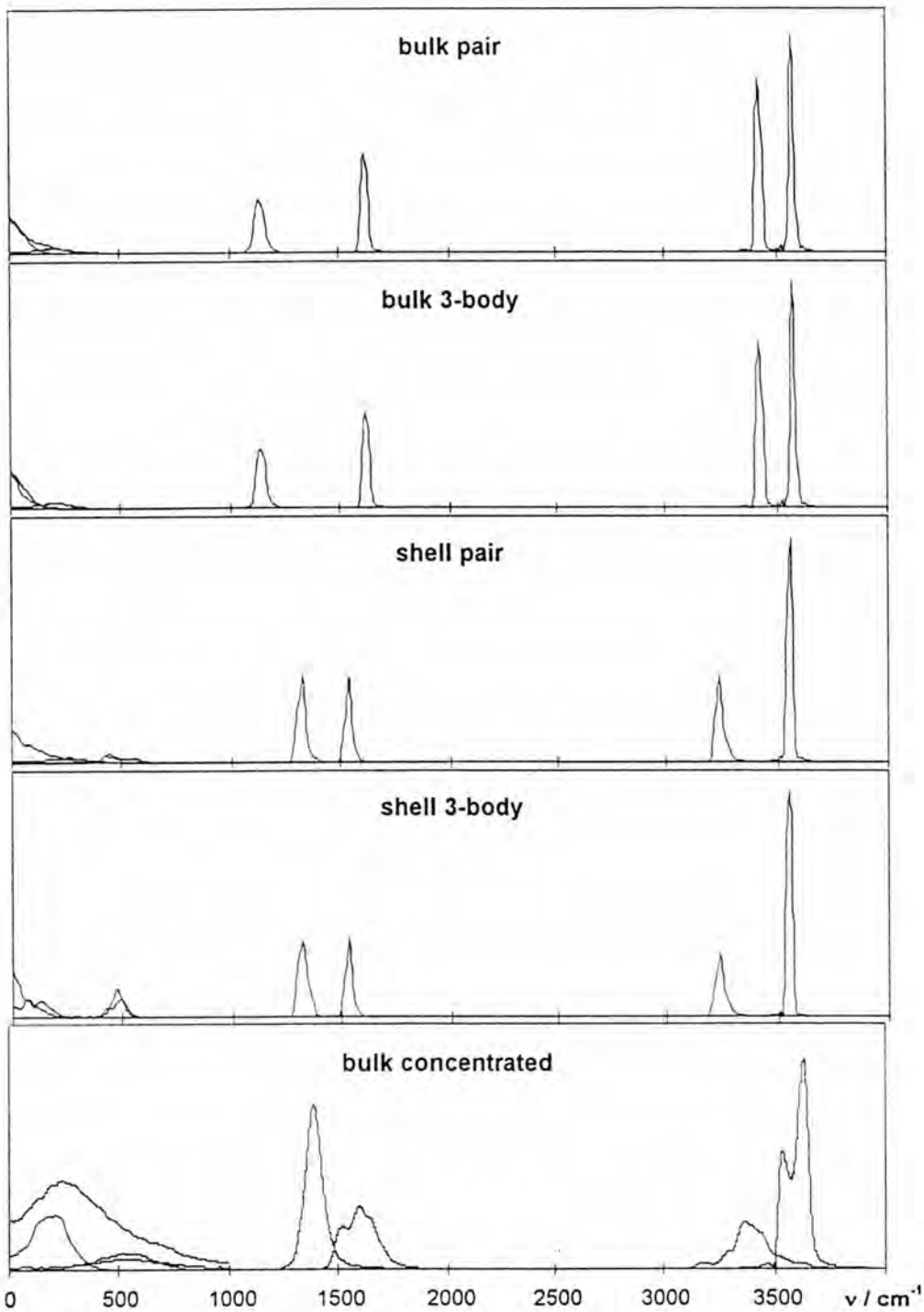

Figure 6.40 Total spectrum densities for ammonia in bulk and in the solvation shell of Ca(II) with and without three-body corrections, and ammonia in concentrated solutions.

The total spectral calculated for wide frequency range are shown in Figure 6.40. The observed spectra can be distinguished into three regions. The intermolecular frequency region, relate to translations and rotations ranging from zero to 700 cm^{-1}, the H-N-H bending region ranging from 700 to 2000 cm^{-1}, and the N-H stretching region ranging from 3000 to 4000 cm^{-1}.